J Nanopart Res (2015) 17:373
DOI 10.1007/s11051-015-3177-0

BRIEF COMMUNICATION

Assembly of graphene oxide on nonconductive nonwovens by the synergistic effect of interception and electrophoresis

Kunyan Jiao · Ting Zhu · Xianhua Li · Mingjing Shan · Zhiwei Xu · Yanan Jiao

Received: 25 May 2015 / Accepted: 8 September 2015 / Published online: 15 September 2015

Abstract Electrophoretic deposition has always been an attractive method to deposit nanoparticles on conductive materials, while most fiber-based materials have poor conductivity which limits the application of electrophoretic deposition in assembling nanoparticles onto fiber-based materials. A new approach to assemble graphene oxide (GO) nanosheets on nonconductive nonwovens via the synergistic effect of electrophoresis and fiber interception was reported in this study. To improve surface wettability, polypropylene (PP) nonwovens were modified by acrylic acid and subsequent N_2 plasma treatment. Then GO nanosheets were anchored onto modified nonwovens by electrophoresis process and nonwoven interception. The results of scanning electron microscopy (SEM) and Fourier transform infrared spectroscopy (FTIR) manifested that etching and grafting simultaneously occurred on the surface of modified PP nonwovens, resulting in a great improvement of nonwoven hydrophily, which corresponded to the results of water contact angle. Furthermore, the results of X-ray diffraction, energy dispersive X-ray, SEM, and FTIR indicated that different amounts of GO nanosheets were successfully assembled onto modified PP nonwovens. This method provides a new avenue for incorporating carbon nanoparticles with nonconductive fiber-based materials, and modified PP nonwovens assembled with GO nanosheets show good air filtration performance for sodium chloride aerosol with a filtration efficiency of 87.9 % and a pressure drop of 36.4 mmH_2O, and the reduced GO/PP composite nonwovens exhibit enhanced conductivity.

Keywords Graphene oxide nanosheet · Nonconductive nonwoven · Interception · Electrophoresis · Air filtration · Conductivity · Surface wettability

K. Jiao · T. Zhu · X. Li · M. Shan · Z. Xu (✉) · Y. Jiao
Key Laboratory of Advanced Braided Composites, Ministry of Education, Tianjin Polytechnic University, Tianjin 300387, People's Republic of China
e-mail: xuzhiwei@tjpu.edu.cn

Introduction

Benefiting from quite high pore volume, interconnected pore structure and high permeability for air and water, fiber-based materials such as fibers, fabrics, and nonwovens, have become potential materials which were applied for filtration (Wang et al. 2012), battery separators (Evanoff et al. 2012), electromagnetic shielding (Haji et al. 2014), energy storage devices, and fuel cells (Hassan et al. 2013). However, most fiber-based materials made of polymer possess poor mechanical, electrical, and thermal properties which limit their application prospect (Gao et al. 2014). With superior performance in electrical, mechanical, and physical properties (Haji et al. 2014; Hsiao et al. 2014), carbon nanoparticles are selected as additives

or reinforcements to enhance the performance and availability of fiber-based materials. Graphene is a marvelous carbon nanomaterial with superlatives of huge specific surface area, electrical, thermal, and mechanical properties (Liu et al. 2011; Yang et al. 2012), as well as energy storage properties (Hu et al. 2013; Li et al. 2011). As a derivative of graphene, graphene oxide (GO) is decorated with carboxyl and carbonyl groups at the edges, and hydroxyl and epoxide functional groups on the basal planes, which makes it strongly hydrophilic and easy to swell and disperse in water (Sun et al. 2012; Zhou et al. 2015). Besides many excellent performance, the good water-dispersibility of GO makes it the preferred choice to be assembled together with fiber-based materials (Liu et al. 2014). The application of fiber-based materials cooperating with carbon nanoparticles has been very extensive (Ju et al. 2008; Xiang et al. 2012).

According to researches previously reported, chemical graft (Einig et al. 2013) and electrophoretic deposition (Guo et al. 2012) have been selected to prepare hybrid of carbon nanoparticles and fiber-based materials. Generally speaking, chemical graft reaction of high-molecular polymer needs relatively harsh reaction conditions, such as catalyst and high temperature, and it is inevitable to cause serious environment pollution and large energy consumption. Electrophoretic deposition is a versatile method in which charged particles in suspension move from one electric pole to another one under the effect of direct current electric field force, and charged particles are deposited on substrate materials (Besra and Liu 2007; Boccaccini et al. 2010; Boccaccini and Zhitomirsky 2002; Chavez-Valdez and Boccaccini 2012). As an environmental friendly and low-cost method, electrophoretic deposition has the advantages of short formation time, simple device, and easy operation (Besra and Liu 2007). Electrophoretic deposition has been regarded as an available technique to deposit carbon nanomaterials on conductive substrates, such as conductive fibers (Boccaccini et al. 2004; Konig et al. 2010; He et al. 2011; Yoshida et al. 2009; Zhitomirsky 1998) and metal substrates (Singh et al. 2013; Lee et al. 2011). Wang and Dryfe (2013) presented a method to prepare the porous hybrid graphene–carbon nanotube layer on the surface of carbon cloth by electrophoretic deposition. Yoshida et al. (2009) formed carbon coating on SiC fiber for two-dimensional composites by electrophoretic deposition. Singh et al. (2013) produced a corrosion-resistant graphene-reinforced composite coating on copper by electrophoretic deposition. Although the researches mentioned above have successfully deposited carbon nanomaterials by electrophoretic deposition, only conductive fiber-based materials have been used as the substrates of electrode (Besra and Liu 2007). However, except for some special conductive fibers such as carbon fibers, most fibers are nonconductive or with weak electrical conductivity, so electrophoretic deposition is rarely used for fiber-based materials to incorporate with carbon nanomaterials. Therefore, more effective and applicable work should be done. By our method, interception and filtration effects of nonwovens were utilized to assist electrophoresis process to incorporate GO nanosheets with nonconductive nonwovens. It is a convenient and feasible approach to assemble GO lamellas onto nonwovens via the synergistic effect of nonwoven interception and electrophoresis, and a few studies have mentioned this method. Polypropylene (PP) nonwovens were selected as the substrates to load GO nanosheets, because of their excellent performance of nontoxicity, resistance to hydrolysis, and low cost (Ramasundaram et al. 2014). While, owning to their low surface energy, PP nonwovens possess poor wettability and adhesion properties, it is extremely necessary to improve the surface property of PP nonwovens through surface modification (Armagan et al. 2014). Plasma techniques have been adopted to improve the surface property of PP nonwovens, and pretreatment by acrylic acid has been utilized to overcome timing effect of plasma treatment after exposure (Černáková et al. 2005).

In this study, PP nonwovens were modified by acrylic acid and subsequent N_2 plasma treatment to enhance the surface wettability and binding force with GO nanosheets. Utilizing filtration and interception of nonwoven with mutually entangled fibrous structure, charged GO nanosheets which moved under electric field force tried to pass through the nonconductive nonwovens, were headed off by the fiber nets and adsorbed on the surface of nonwoven fibers. By this method, the pore structure of nonconductive nonwovens and electrophoresis were creatively combined to make modified PP/GO-composited nonwovens, and the as-prepared materials showed good performance in air filtration and conductivity.

Experimental

Materials

PP nonwovens (basis weight 50 g/m^2) were provided by Tianjin Teda Co., Ltd. China. Acrylic acid was purchased from Tianjin FuChen Chemical Reagent Co., Ltd. China. Potassium permanganate, sulfuric acid and hydrogen peroxide were provided by Tianjin Fengchuan Chemical Reagent Co., Ltd. China. Hydrazine hydrate was purchased from Sigma-Aldrich Co. Korea. All reagents used in the experiment were without further purification.

Preparation of GO

Improved Hummers' method (Shi et al. 2012) was used to prepare graphite oxide. A 9:1 mixture of concentrated H_2SO_4/H_3PO_4 (360:40 ml) was added to a mixture of 3.0 g graphite flakes and 18.0 g $KMnO_4$. The reactant was then heated to 50 °C and stirred for 24 h. The reactants were cooled to room temperature and poured onto ice (400 ml) with 30 % H_2O_2 (3 ml). Subsequently, the mixture was centrifuged and the supernatant was decanted away. Meanwhile, the mixture was washed with an aqueous hydrochloric acid solution (10 vol.%) to remove the sulfate ions and then washed repeatedly with distilled water until pH = 7. The graphite oxide slurry was freeze-dried (−50 °C) for 48 h (Shi et al. 2012). By ultrasonication of graphite oxide aqueous solution, we could get GO with high interlayer spacing and exfoliation (Singh et al. 2013). To form homogeneous colloidal suspensions, 0.5, 1, and 2 g/l GO aqueous dispersion was prepared by ultrasonic treatment for 3 h, respectively.

Modification of PP nonwovens

In brief, PP nonwovens were modified by acrylic acid and N_2 microwave plasma treatment. Firstly, PP nonwovens were pretreated by 30 % acrylic acid aqueous solution with a water bath of 60 °C for 1.5 h and dried at 60 °C. Then, the pretreated PP samples were placed on the plate of the plasma chamber which was evacuated to 5 Pa at room temperature. Thereafter, N_2 was passed into the chamber with a gas flow rate of 1.0 l/h to keep a pressure of 40 Pa. N_2 microwave plasma treatment was performed on YZ-2 microwave plasma generator, and the treatment degree was adjusted by changing time and power of plasma. The samples pretreated by acrylic acid are operated at the conditions described in Table 1. And the plasma power was set for 60, 90, 150, and 200 W, and the treatment time was set for 3, 6, and 9 min, respectively. The sample treated by N_2 plasma at 90 W for 6 min was denominated as PP 90-6, and the denominations of other samples are listed in Table 1.

Assembly of GO onto PP nonwovens

Two same stainless steel plates were selected as electrode substrates to suppress the formation of metal hydroxides and vertically placed in the electrophoresis tank. The pristine and modified PP nonwovens (15 × 15 cm^2) were vertically fixed between the stainless steel plates and nearly approached to the anode substrate. Electrophoresis experiments were carried out at direct current voltages of 24 V, deposition time of 20 min, and electrode distance of 8 cm. Because of carrying with carboxyl and carbonyl functional groups, GO was highly negatively charged (Fugetsu et al. 2010) and moved from cathode electrode to anode electrode (Besra and Liu 2007). After electrophoresis process, the nonwovens were rinsed by distilled water to remove GO nanosheets slightly floated on the surface, and then put in the oven at 60 °C. In detail, 0.5, 1 and 2 g/l GO aqueous solutions were used to incorporate with modified PP nonwovens (PP 90-6) by electrophoresis process, which were denoted as M-PP/GO-0.5, M-PP/GO-1,

Table 1 Experiment conditions of N_2 plasma treatment for PP nonwovens pretreated by acrylic acid

Samples	Treatment time (min)	Treatment power (W)
PP 60-3	3	60
PP 60-6	6	
PP 60-9	9	
PP 90-3	3	90
PP 90-6	6	
PP 90-9	9	
PP 150-3	3	150
PP 150-6	6	
PP 150-9	9	
PP 200-3	3	200
PP 200-6	6	
PP 200-9	9	

and M-PP/GO-2, respectively. As comparison, 1 g/l GO aqueous solution was assembled onto pristine PP nonwovens by electrophoresis process or onto modified PP nonwovens by simple dipping method, noted as PP/GO-1 and M-PP/GO-1-dipping, respectively. Moreover, the M-PP/GO-composited nonwoven was chemically reduced by hydrazine hydrate as the paper reported (Ramasundaram et al. 2014), which was noted as M-PP/rGO. The preparation route and proposed formation mechanism of modified PP/GO nonwovens and the schematic diagram of electrophoresis process are shown in Fig. 1a–b.

Characterization

Transmission electron microscopy (TEM, FEITecnai F30, operated at 300 kV) with a high resolution was utilized to observe the microstructure and morphology of the GO nanosheets. Then, X-ray Diffraction (XRD, Burker D8 Discover) with Cu Kα radiation ($\lambda = 1.54059$ Å) was used to reveal the structure of GO, modified PP nonwovens, and modified PP/GO nonwovens at a scanning speed of 5/min from 3 to 60°. The morphology and thickness of GO were observed by AFM (CSPM5500) under the tapping mode. The zeta potential of GO dispersion was measured by Delsa Nano C Particle Analyzer (Beckman Coulter Company, America). And the morphologies of pristine PP nonwoven and multi-scale modified PP/GO nonwovens were examined by field emission scanning electron microscopy (FE-SEM) (S-4800, Hitachi, Japan). Elemental composition analyses were carried out by an energy dispersive X-ray (EDX) spectrometer equipped on FE-SEM. Each sample was coated with a thin layer of gold (~5 nm) before observing. The water contact angle (CA) measurements were performed using a CA measurement apparatus (JYSP-180 Contact Angle Analyzer) according to the sessile-drop method (Yue et al. 2015). Briefly, a water droplet was deposited on a flat nonwoven surface, and the CA of the droplet with the surface was measured. The instantaneous water CA obtained within 0.5 s (ensuring observable vibration of the liquid drop on the solid sample had already ceased) was recorded. Each final water CA value was obtained by averaging over more than five water CA values of different spots. And to guarantee the accuracy of experimental results, each water CA measurement was conducted five times to acquire the average data and the standard deviation. Fourier transform infrared spectroscopy (FTIR) was acquired using a Bruker Tensor 27 system in the 3800–800 cm^{-1} wavenumber range to analyze the functional groups grafted onto PP nonwovens. All the samples were pressed into a pellet with potassium bromide (KBr) before measurement.

The filtration efficiency and air flow resistance (pressure drop in mmH_2O column height) were measured by an automated filter tester TSI 8130 (TSI incorporation, America). The TSI 8130 could deliver neutralized micron monodisperse solid sodium chloride aerosol (NaCl, a mass median diameter of 0.5 μm, and a geometric standard deviation not exceeding 2.83), and NaCl aerosols were fed into a

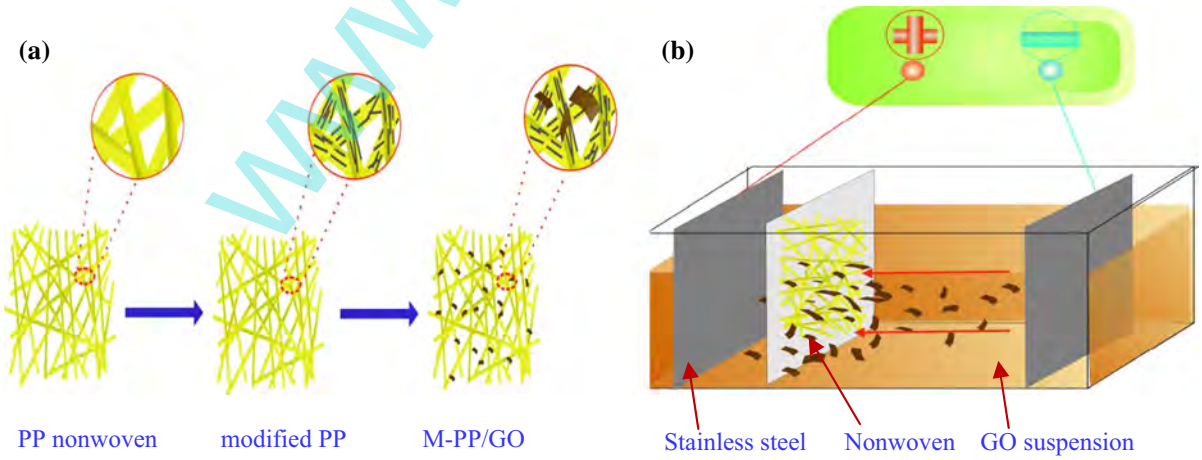

Fig. 1 **a** Schematic illustration of fabrication of M-PP/GO nonwovens, **b** schematic diagram of electrophoresis process

filter holder with an effective area of 100 cm^2. All filtration tests were conducted with a continuous air flow of 32 l/min at room temperature. Conductivity measurements were demonstrated using Alpha-A high-resolution conductivity measurement system with the frequency range from 0.1 Hz to 10 MHz at room temperature.

Results and discussion

Characterization of GO and M-PP/GO

Figure 2a–b shows the TEM and high-resolution TEM images of the GO nanosheets. The results revealed that the GO nanosheets with transparent flake-like shape were of few layers on the porous copper and high-resolution TEM also indicated the perfect structure of GO (Fig. 2b). As shown in Fig. 2c, the GO nanosheets were mainly consisted of mono-layer GO platelets. Figure 2d indicates that the thicknesses of GO nanosheets were mostly within a range of 1.15–1.5 nm, which were about slightly thicker than that of mono-layer GO nanosheet previously reported due to the extensive oxidation during the preparation process. And the zeta potential results showed that the GO suspensions with different concentrations are greatly negatively with zeta potential from −28.04 to −50.21 mV (Fig. 2e). In general, the zeta potential confers the degree of repulsion between charged particles in dispersion, and a high zeta potential (negative or positive above 40 mV) is an indicator that the dispersion resists aggregation and consequently remains stable (Zhang et al. 2013b).

The XRD spectra of pristine PP, modified PP, and modified PP/GO nonwovens, as well as the GO nanosheets were performed (Fig. 2f). From the XRD spectrum of GO, the intensity and diffraction angle of the peak (at approximately 10.6°) represented the interlayer spacing of GO nanosheets, which indicated that graphite was successfully oxidized (Liu et al. 2011). As for another two tiny bands at 26° and 43°,

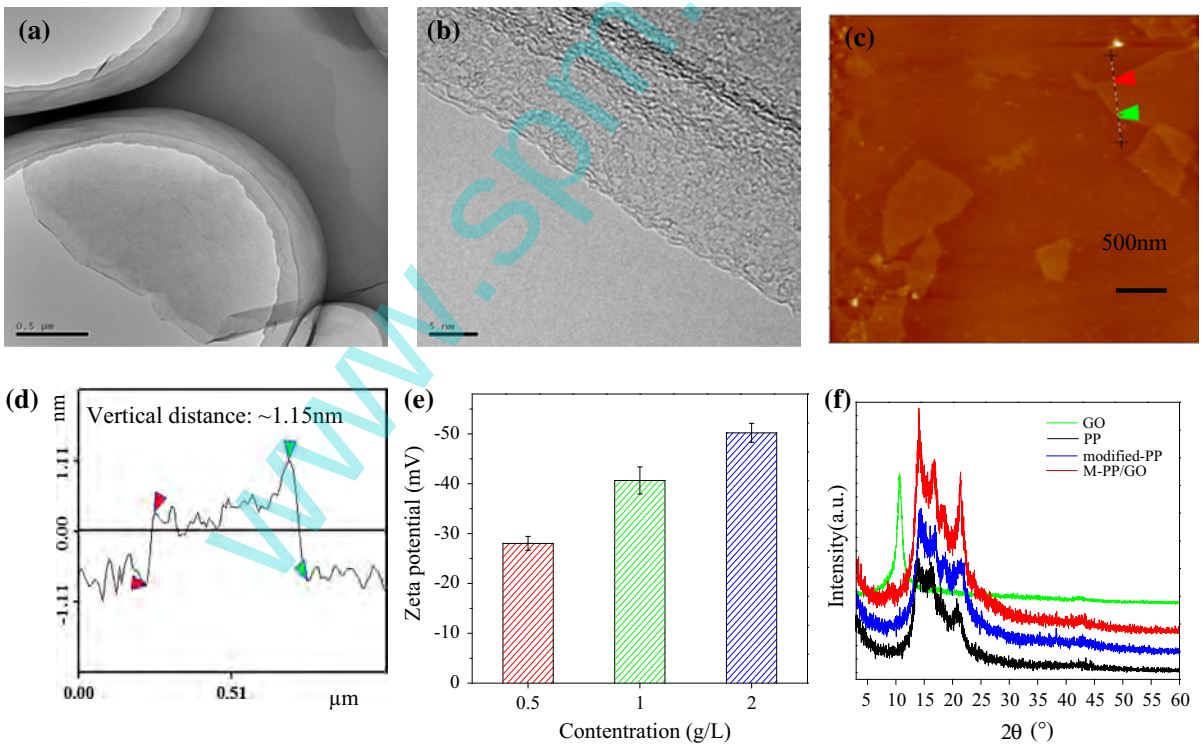

Fig. 2 **a, b** The TEM and high-resolution TEM of GO nanosheets, **c** tapping mode AFM topographic image of GO nanosheets and **d** AFM cross-section of GO nanosheets, **e** the zeta potential of GO suspensions with different concentrations and **f** the XRD spectra of GO, PP, modified PP, and M-PP/GO nonwovens

they were correlated with the rather limited ordering for the limited few layers in GO and the turbostratic band of disordered carbon materials, respectively (Chen et al. 2011). As indicated in the XRD spectra of PP, modified PP, and M-PP/GO (1 g/l GO aqueous solution was used to assemble GO on the modified PP nonwovens by electrophoresis process), four distinct diffraction peaks were appeared at 2θ value of 14.159°, 16.747°, 18.026°, and 21.324° corresponding to the (100), (040), (130), and (131) crystal planes diffraction peaks of PP, respectively. Moreover, the M-PP/GO showed a weak peak at 9.17° which responded to the characteristic peak of GO at 10.6°. It may be because the crystal behavior of PP affected the peak intensity and position, and made it weaker and shift to the left. The XRD results indicated that acrylic acid and plasma treatment have no effect on the structure of PP nonwovens, and GO nanosheets were successfully assembled on the modified PP nonwovens.

Hydrophily of nonwovens

The water CA is an important parameter to measure surface hydrophily, which is one of the most important properties of modified PP nonwovens. Good hydrophily could influence the surface energy of PP nonwovens and enhance the adhesion with GO nanosheets. In general, a smaller water CA corresponds to a more hydrophilic material. The water CA measured immediately after water was dropped onto the samples would preferably reflect the natural wettability of the materials (Zhang et al. 2013a). As shown in Fig. 3a, the functional relation between the water CA and the plasma treatment power was demonstrated. With the enhancement of plasma treatment power, the water CA of samples decreased first but then increased. The reason was that low plasma power (60 W) was too difficult to motivate active particles, while excessive plasma power would cause overheating (this plasma is a cold type), so only the power in an appropriate range, plasma could make active particles and be more benefit for the hydrophily improvement of modified PP nonwovens (Lopez et al. 2012). Similarly, water CA decreased sharply at first but then increased slightly with the time of plasma treatment prolonging (Fig. 3b). In detail, the pristine PP nonwovens possess a hydrophobic behavior with a water CA of 125°. Pretreated by acrylic acid, the water CA of the PP samples decreased to 106°. Once treated by N_2 plasma, the water CA was less than 90°, indicating that modified PP nonwovens became hydrophilic. It was significant to remind that the water CA of PP 90-6 nonwovens reached a minimum of 20° and the sample showed a marked hydrophilic behavior. It was etching onto fibers and the introduction of oxygen functional group that made nonwovens hydrophilic. However, with the power and time increasing, the CA increased instead and the wettability of samples declined slightly. That may be because long exposure time made cold type plasma produced local overheating, which was bad for the etching of fibers. On the whole, etching and the introduction of oxygen functional groups simultaneously worked to improve the hydrophilic properties of M-PP nonwovens, which were in accordance with the results of SEM and FTIR. As shown in Fig. 3c, difference in the decaying rate of pristine PP and modified PP nonwovens showed obviously enhanced water diffusing in 10 s determination. And with the time extending to 10 s, the water CA became lower compared with the instantaneous water CA when the water drop dripped on the surface of samples, implying the good water affinity and improved hydrophily of modified PP nonwovens (Zhang et al. 2013b).

Surface morphology of nonwovens

Surface morphology of the pristine and modified PP nonwovens was characterized by FE-SEM (Fig. 4). Because of the best hydrophily of modified PP nonwovens, the plasma power was set up at 90 W for the subsequent tests. As can be seen in Fig. 4a, the surface of pristine PP nonwoven was extremely smooth. The PP samples only pretreated by acrylic acid showed slightly convex surface and distributed with a few white dots (Fig. 4b). Figure 4c manifests the surface morphology of PP 90-3 (as noted in Table 1), and many raised spots were distributed on the surface of PP nonwovens which were slightly hydrophilic. The fiber surface of PP 90-6 became rough, and some traces of obvious strips etching were also observed (Fig. 4d). Figure 4e shows the SEM photograph of PP 90-9, and small dots (with average size in the 0.1–0.5 μm range) derived from the etching

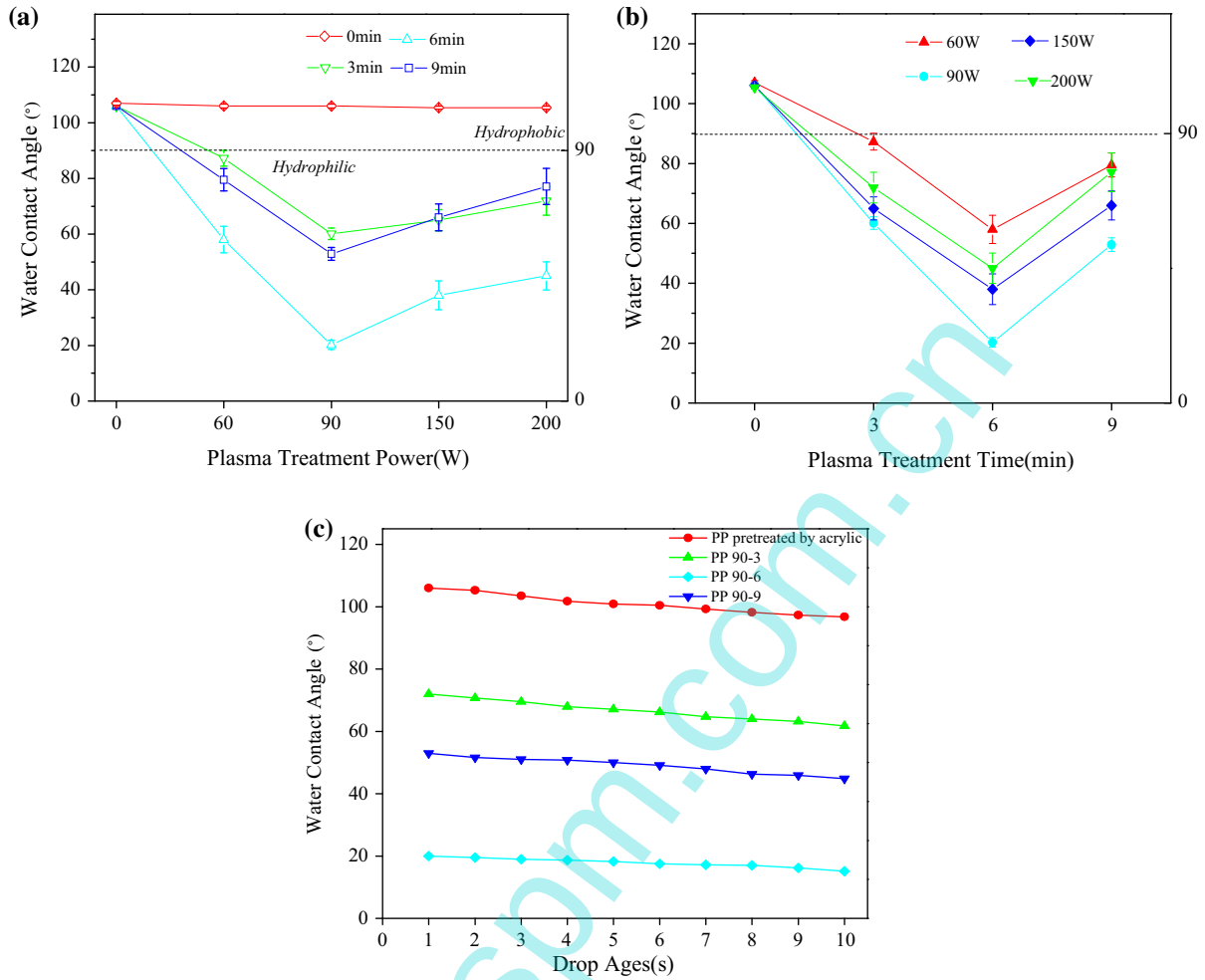

Fig. 3 The water CA as functions of **a** plasma treatment power, **b** plasma treatment time, and **c** decay of water CA as a function of time

process can be detected. The active plasma species continuously bombard the fiber surface and the tiny dots might be formed by nondirectional ablation or re-deposition of etched substances (Man et al. 2014). Clearly, the fiber surface of PP 90-6 was rougher, and owned more adhered dots and deeper trench compared with that of PP 90-3 and PP 90-9. For short treatment time, plasma was difficult to cause etching, and for long exposure time (longer than 6 min), the plasma produced local overheating, which went against the etching of polymer fibers and caused some degradation effects. Once high energy particles of plasma bombarded the surface of PP fibers, energy transfer occurred and this process produced a large number of free radicals. Adjacent PP polymer-free radicals may be complex and crosslink, and polymer may be dehydrogenated to form a double bond or other new functional groups, such as carbonyl and carboxyl. In this experiment, surface radicals generated by the N_2 plasma activation worked as reactive species to graft acrylic acid.

FTIR spectra of nonwovens

Figure 5 shows the FTIR spectra of pristine PP, modified PP nonwovens under different plasma treatment times (denominated as Table 1), and GO nanosheets, as well as the M-PP/GO (the modified PP 90-6 nonwoven incorporated with 1 g/l GO by electrophoresis process). The formation of some functional groups played an important role in

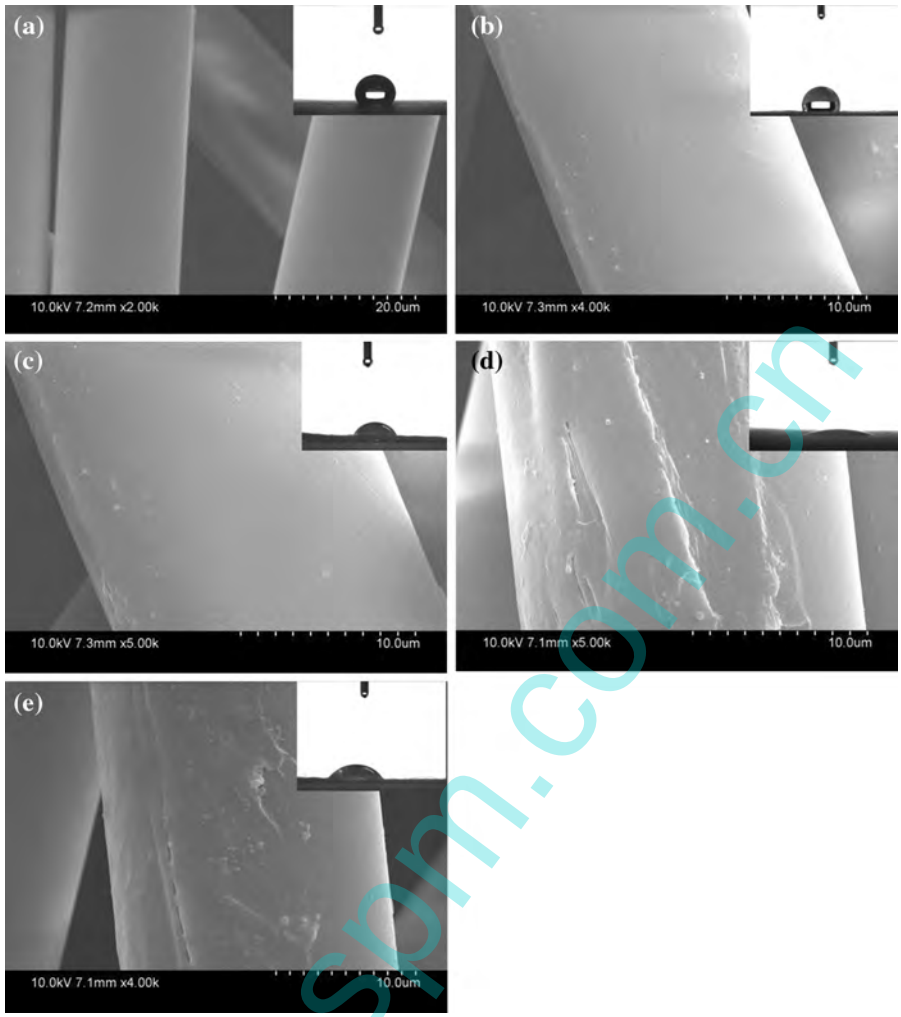

Fig. 4 Surface morphology of pristine and modified PP nonwoven fibers and the *insert* showed a drop of water on the surface of PP nonwovens: **a** pristine PP nonwoven, **b** PP nonwoven pretreated by acrylic acid, **c** PP 90-3 nonwoven, **d** PP 90-6 nonwoven, and **e** PP 90-9 nonwoven

enhancing the hydrophilic properties of the PP nonwovens. Form FTIR spectrum of pristine PP, the peaks between 2950 and 2800 cm^{-1} corresponded to the various aliphatic C–H stretching modes, and the peaks near 1450 and 1380 cm^{-1} were the CH_2 and CH_3 deformation bands, respectively. The major peak of the carbonyl (C=O) stretching band at 1725 cm^{-1}, C–O band at 1247 cm^{-1}, and the broad absorption band of hydroxy (O–H) at 3300–3500 cm^{-1} manifested that acrylic acid was successfully grafted onto the fiber surface of PP 60-3, PP 60-6, and PP 60-9 nonwovens (Černáková et al. 2005), which could indicate that the N_2 plasma activation accelerated the graft and led to a high retention of acrylic acid on PP fiber surface. In the FTIR spectra of M-PP/GO and GO, the peaks of the C=O, O–H, and C–O were presented at the corresponding position. Moreover, a small peak associated with aromatic C=C at 1620 cm^{-1} also appeared, which was not existed in the FTIR spectra of modified PP nonwovens, indicating the successful assembly of GO nanosheets onto modified PP nonwovens (Ramasundaram et al. 2014). The conclusion of FTIR analysis was in accordance with the results of SEM and hydrophily characterization.

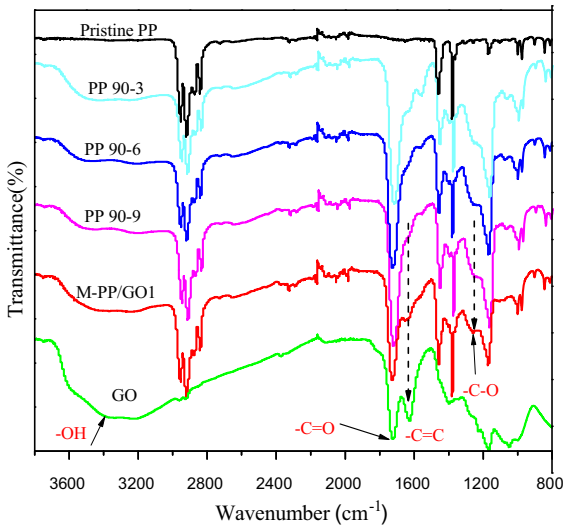

Fig. 5 The FTIR spectra of pristine PP, modified PP nonwovens, GO nanosheets, and M-PP/GO nonwovens

Surface morphology and EDX analysis of nonwovens

Pristine PP and PP 90-6 nonwovens were selected to fabricate PP/GO-composited nonwovens by simply dipping or the electrophoresis process. Figure 6 shows that the GO lamellas were assembled onto the surface of PP nonwovens and PP fibers retained original morphology, which indicated that the fiber structure was not cracked during dipping or electrophoresis process. Figure 6a indicates the surface morphology of M-PP/GO-1-dipping and only a small quantity of GO nanosheets were assembled onto PP fibers. Figure 6b shows the surface morphology of PP/GO-1 and GO lamellas were lightly lapped on the fibers, indicating the poor adhesion between pristine PP fibers and GO nanosheets. Figure 6c–d displays the morphology of M-PP/GO-0.5 and only a few GO layers were decorated on modified fibers, covered by a piece of GO nanosheets. As can be seen in Fig. 6e–f, M-PP/GO-1 fibers covered by GO nanosheets became wrinkled and coarse (Ramasundaram et al. 2014), and the GO nanosheets warped up and winded on the fibers and pieces of GO nanosheets stretched perpendicularly to the fiber axial. Clearly, the wrinkles and folds of GO nanosheets decorated on fibers became more prominent after the GO concentration was enhanced to 2 g/l (Fig. 6g). Obviously, the increase of concentration made the GO easy to agglomerate and pieces of GO nanosheets congregated onto a small amount of fibers (Fig. 6h). The improvement of hydrophily enhanced the inter-molecular forces between modified PP fibers and the GO, making nonwovens prone to intercept and anchor GO nanosheets which moved under the electric field force. In the electrophoresis process, negatively charged GO nanosheets moving from negative electrode to positive electrode were intercepted by the intertwined fibrous

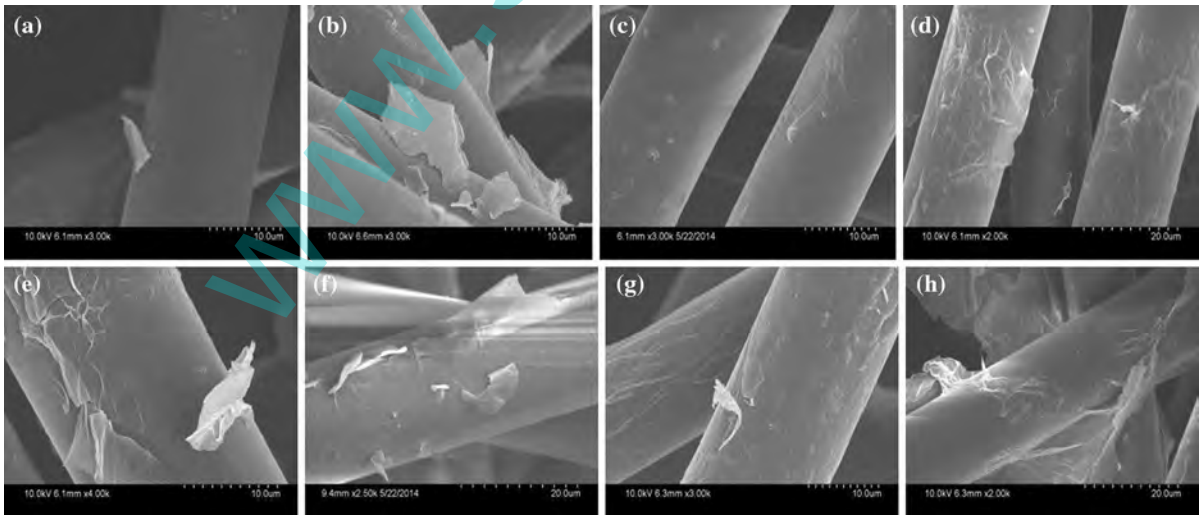

Fig. 6 The SEM images with different magnifications of PP/GO nonwovens fabricated by dipping or electrophoresis process: **a** M- PP/GO-1-dipping, **b** PP/GO-1, **c**- **d** M-PP/GO-0.5, **e**- **f** M-PP/GO-1, and **g**- **h** M-PP/GO-2

nonwovens placed between the opposite electrodes, and fitly anchored on the fiber surface. Thus, the electrophoresis and nonwoven interception suitably worked together and both of them were indispensable in the fabrication of modified PP/GO nonwovens.

Figure 7 signifies the SEM images, SEM-EDX spectra analysis, and the carbon and oxygen atomic percentage (at.%) of pristine PP, GO nanosheets, modified PP, and M-PP/GO nonwovens. The successful incorporation of GO nanosheets and PP nonwovens was confirmed by the SEM and EDX spectra. As is known to all, PP is composed of carbon and hydrogen, while the surface of the modified PP (M-PP) nonwovens contained a small amount of oxygen (5.45 at.%) due to the introduction of oxygen-containing functional groups by acrylic acid grafting and plasma treatment (Fig. 7a1–a2). Figure 7b1–b2 shows the surface morphology and EDX spectra of GO nanosheets which possessed plenty of creases and wrinkle, and rich oxygen-containing functional groups making the oxygen content up to 42.13 %. For comparison, the M-PP/GO-1-dipping and PP/GO-1 were measured by the SEM-EDX spectra, and the oxygen atomic contents were 8.29 and 11.08 % (Fig. 7c_1–c_2, d_1–d_2). Figure 7e_1–g_1,e_2–g_2 illustrates the SEM images with low magnification and the EDX spectra of M-PP/GO-0.5, M-PP/GO-1, and M-PP/GO-2, and the oxygen atomic content, were 16.73, 17.57, and 18.58 %, respectively (Fig. 7h). Owning to the combined action of the surface modification and electrophoresis process, the atomic ratio values of oxygen and carbon of M-PP/GO-1 raised 1.3 and 0.72 times comparing with that of M-PP/GO-1-dipping and PP/GO-1. The results indicated the successful assembly of GO nanosheets with different contents onto modified PP nonwovens by the synergistic effect of interception and electrophoresis.

Air filtration performance of nonwovens

The filtration efficiency and pressure drop are the key parameters of fibrous filters, and a combination of high filtration efficiency and low pressure drop is an evaluation criteria for a good filter (Li et al. 2014). As shown in Fig. 8, the introduction of GO nanosheets enhanced the filtration performance of nonwovens and

Fig. 7 The SEM images and SEM-EDX spectra analysis of samples: **a1–a2** M-PP, **b1–b2** GO nanosheets, **c1–c2** M-PP-GO-1-dipping, **d1–d2** pristine PP/GO, **e1–e2** M-PP/GO-0.5, **f1–f2** M-PP/GO-1, **g1–g2** M-PP/GO-2, and **h** the carbon and oxygen atomic concentrations of pristine PP, GO nanosheets, M-PP, and M-PP anchored with GO nanosheets determined by the EDX spectra

the M-PP/GO-1 nonwoven showed a filtration efficiency of 87.9 % and a pressure drop of 36.4 mmH_2O. In detail, although the air filtration resistance of PP nonwovens assembled with GO nanosheets was slightly increased, the filtration efficiency had a significant improvement. The filtration efficiency of M-PP/GO-1 doubled, while the pressure drop increased less than 10 % comparing with that of pristine PP nonwovens. In addition, the filtration efficiency of M-PP/GO-1 enhanced 38.2 and 36.9 %, and the pressure drop increased 8.8 and 4.6 % comparing with that of M-PP/GO-1-dipping and PP/GO-1 nonwovens, which reflected good filtration performance of the modified PP nonwovens covered with GO nanosheets by electrophoresis process. The assembly of GO nanosheets enlarged surface roughness and specific surface area of the modified nonwovens and thus finally enhanced the filtration performance.

Conductive performance of nonwovens

The conductive performance of pristine PP, M-PP/GO, and M-PP/rGO nonwovens (chemically reduced by hydrazine hydrate), is illustrated in Fig. 9. The conductivity of nonwovens was enhanced with the increase of frequency in range from 0.1 to 10^7 Hz. Obviously, the conductivity of M-PP/rGO nonwovens (3.0×10^{-6} S/m at the frequency of 10^5 Hz) rapidly increased duo to the reduction of GO nanosheets, which was improved about 20 and 50 times compared with that of M-PP/GO (1.5×10^{-7} S/m) and pristine PP nonwovens (6.0×10^{-8} S/m), respectively. And with the frequency increasing to 10^6 Hz, the conductivity of M-PP/rGO enhanced to 3.0×10^{-5} S/m, reaching the anti-static criterion (10^{-6} S/m) (Liu et al. 2014), which is about two orders of magnitude higher than that of PP nonwovens.

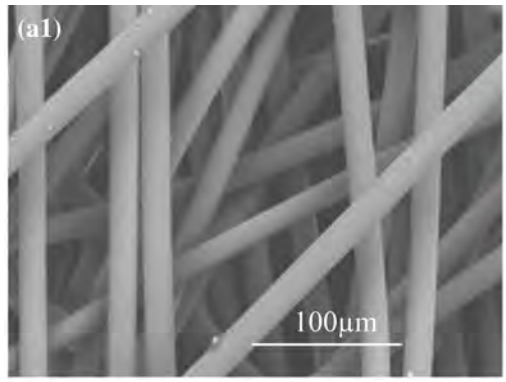

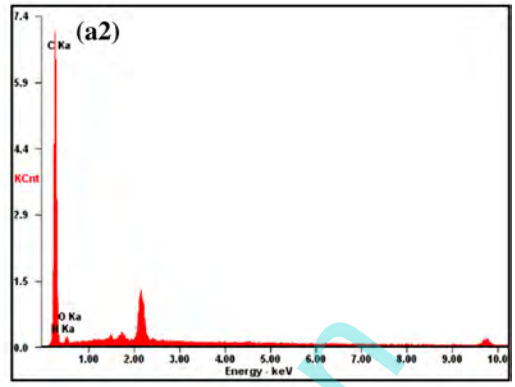

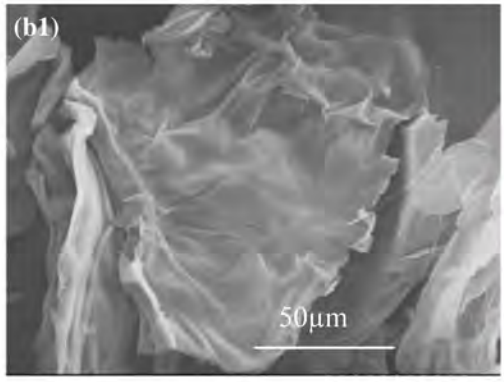

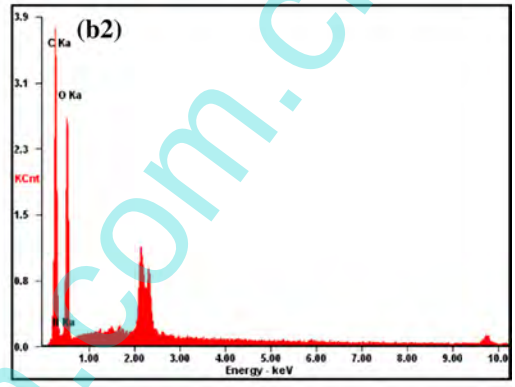

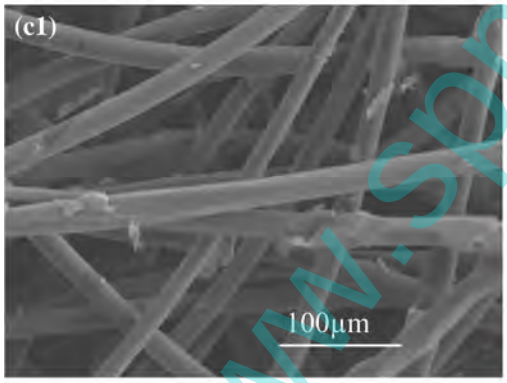

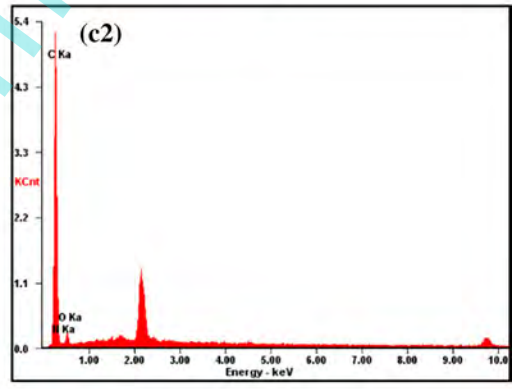

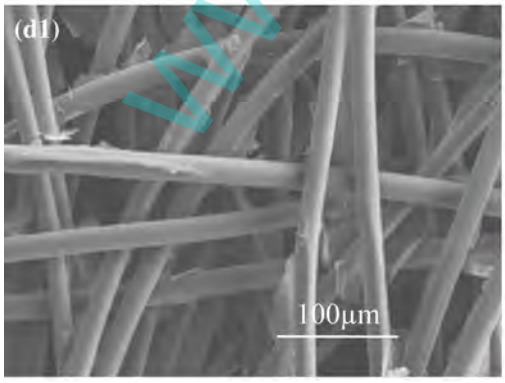

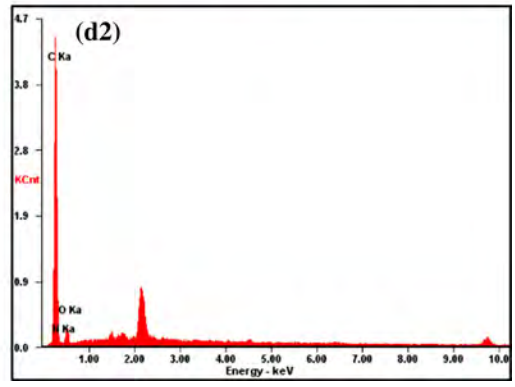

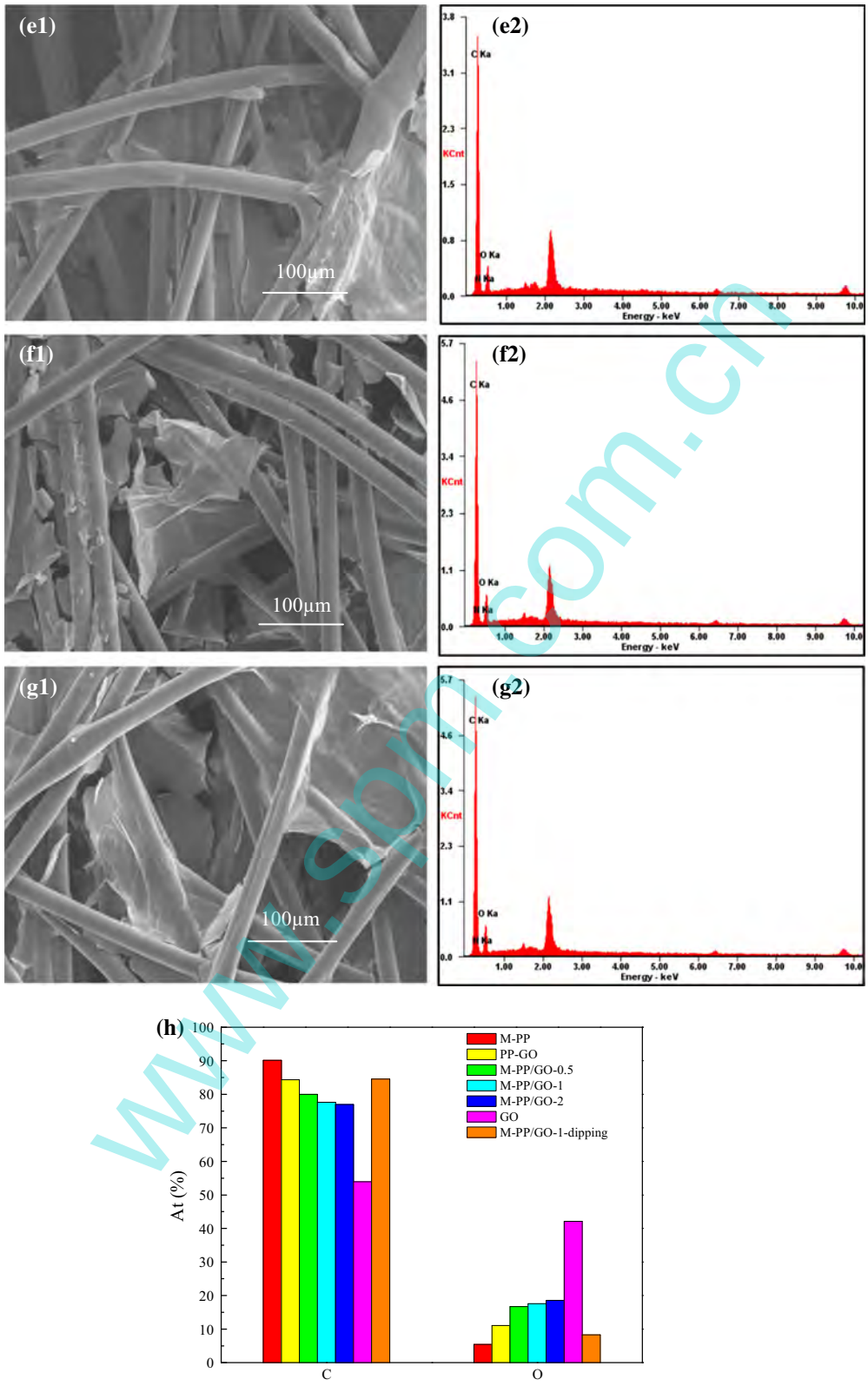

Fig. 7 continued

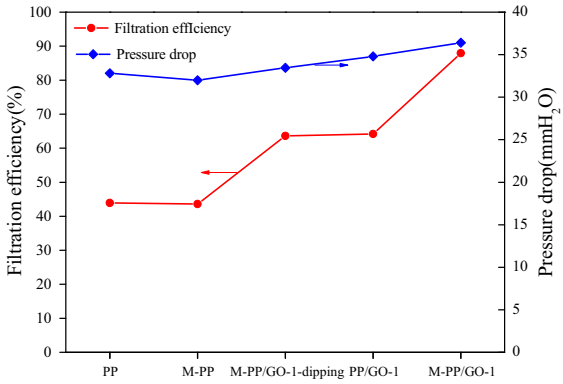

Fig. 8 The filtration performance of pristine PP, modified PP, and PP nonwovens incorporated with GO nanosheets

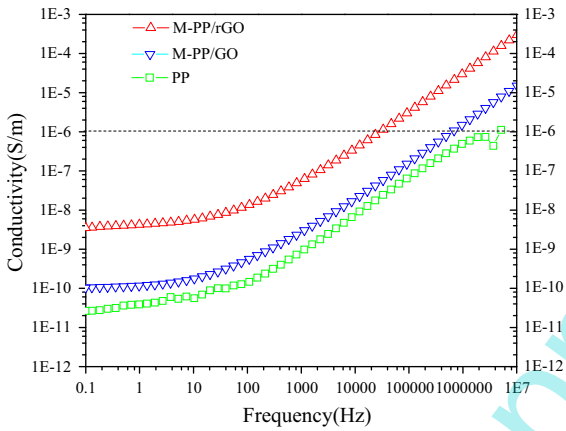

Fig. 9 The conductivity of nonwovens as a function of frequency at room temperature

Conclusions

In summary, an approach to incorporate GO nanosheets with nonconductive nonwovens was taken by the synergistic effect of electrophoresis and nonwoven interception. After the modification of nonwovens by acrylic acid and N_2 plasma treatment, the surface wettability and adhesion between fibers and GO lamellas have been significantly enhanced, demonstrated by the decrease of water CA and the increase of fiber roughness. The results of FTIR spectra indicated that carbonyl and carboxyl groups were introduced onto modified fibers, and the GO nanosheets were firmly anchored onto the fiber surface. The results of SEM and EDX indicated that GO nanosheets with different amounts were successfully assembled onto modified PP nonwovens by the synergistic effect of interception and electrophoresis. The composite nonwovens assembled with GO nanosheets showed good performance in air filtration and PP nonwovens incorporated with reduced GO exhibited enhanced conductivity. The presented method greatly expands the application field of electrophoresis in the modification of nonconductive fiber-based materials.

Acknowledgments The work was funded by the National Natural Science Foundation of China (51408416) and the Petrochemical Joint Funds of National Natural Science Fund Committee—China National Petroleum Corporation (U1362108).

References

Armagan OG, Kayaoglu BK, Karakas HC, Guner FS (2014) Adhesion strength behaviour of plasma pre-treated and laminated polypropylene nonwoven fabrics using acrylic and polyurethane-based adhesives. J Ind Text 43:396–414. doi:10.1177/1528083712458303

Besra L, Liu M (2007) A review on fundamentals and applications of electrophoretic deposition (EPD). Prog Mater Sci 52:1–61. doi:10.1016/j.pmatsci.2006.07.001

Boccaccini AR, Zhitomirsky I (2002) Application of electrophoretic and electrolytic deposition techniques in ceramics processing. Curr Opin Solid State Mater Sci 6:251–260. doi:10.1016/s1359-0286(02)00080-3

Boccaccini AR, Karapappas P, Marijuan JM, Kaya C (2004) TiO_2 coatings on silicon carbide and carbon fibre substrates by electrophoretic deposition. J Mater Sci 39:851–859. doi:10.1023/B:JMSC.0000012914.47793.3e

Boccaccini AR, Keim S, Ma R, Li Y, Zhitomirsky I (2010) Electrophoretic deposition of biomaterials. J R Soc Interface 7:S581–S613. doi:10.1098/rsif.2010.0156.focus

Černáková L, Kováčik D, Zahoranová A, Černák M, Mazúr M (2005) Surface modification of polypropylene non-woven fabrics by atmospheric-pressure plasma activation followed by acrylic acid grafting. Plasma Chem Plasma Process 25:427–437. doi:10.1007/s11090-004-3137-4

Chavez-Valdez A, Boccaccini AR (2012) Innovations in electrophoretic deposition: alternating current and pulsed direct current methods. Electrochim Acta 65:70–89. doi:10.1016/j.electacta.2012.01.015

Chen L et al (2011) Reduction and disorder in graphene oxide induced by electron-beam irradiation. Mater Lett 65:1229–1230. doi:10.1016/j.matlet.2011.01.063

Einig A, Rumeau P, Desrousseaux S, Magga Y, Bai JB (2013) Plasma polymerized thin coating as a protective layer of carbon nanotubes grafted on carbon fibers. J Phys 429:012051. doi:10.1088/1742-6596/429/1/012051

Evanoff K, Benson J, Schauer M, Kovalenko I, Lashmore D, Ready WJ, Yushin G (2012) Ultra strong silicon-coated carbon nanotube nonwoven fabric as a multifunctional lithium-ion battery anode. ACS Nano 6:9837–9845. doi:10.1021/nn303393p

Fugetsu B, Sano E, Yu H, Mori K, Tanaka T (2010) Graphene oxide as dyestuffs for the creation of electrically conductive fabrics. Carbon 48:3340–3345. doi:10.1016/j.carbon.2010.05.016

Gao J, Li W, Shi H, Hu M, Li RKY (2014) Preparation, morphology, and mechanical properties of carbon nanotube anchored polymer nanofiber composite. Compos Sci Technol 92:95–102. doi:10.1016/j.compscitech.2013.12.008

Guo J, Lu C, An F, He S (2012) Preparation and characterization of carbon nanotubes/carbon fiber hybrid material by ultrasonically assisted electrophoretic deposition. Mater Lett 66:382–384. doi:10.1016/j.matlet.2011.09.022

Haji A, Rahbar RS, Shoushtari AM (2014) Improved microwave shielding behavior of carbon nanotube-coated PET fabric using plasma technology. Appl Surf Sci 311:593–601. doi:10.1016/j.apsusc.2014.05.113

Hassan MA, Bong Yeol Y, Wilkie A, Pourdeyhimi B, Khan SA (2013) Fabrication of nanofiber meltblown membranes and their filtration properties. J Membr Sci 427:336–344. doi:10.1016/j.memsci.2012.09.050

He S et al (2011) Polyimide nano-coating on carbon fibers by electrophoretic deposition. Colloid Surf A-Physicochem Eng Asp 381:118–122. doi:10.1016/j.colsurfa.2011.03.039

Hsiao ST et al (2014) Lightweight and flexible reduced graphene oxide/water-borne polyurethane composites with high electrical conductivity and excellent electromagnetic interference shielding performance. ACS Appl Mater Interfaces 6:10667–10678. doi:10.1021/am502412q

Hu Y, Li X, Wang J, Li R, Sun X (2013) Free-standing graphene–carbon nanotube hybrid papers used as current collector and binder free anodes for lithium ion batteries. J Power Sources 237:41–46

Ju YW, Choi GR, Jung HR, Lee WJ (2008) Electrochemical properties of electrospun PAN/MWCNT carbon nanofibers electrodes coated with polypyrrole. Electrochim Acta 53:5796–5803. doi:10.1016/j.electacta.2008.03.028

Konig K, Novak S, Ivekovic A, Rade K, Meng D, Boccaccini AR, Kobe S (2010) Fabrication of CNT-SiC/SiC composites by electrophoretic deposition. J Eur Ceram Soc 30:1131–1137. doi:10.1016/j.jeurceramsoc.2009.07.027

Lee W, Lee SB, Yi JW, Kim BS, Byun JH (2011) Fabrication of carbon nanotube/copper hybrid nanoplatelets coated carbon fiber composites by thermal vapor and electrophoretic depositions. Electrochem Solid-State Lett 14:K37–K39. doi:10.1149/1.3582354

Li P, Wang C, Zhang Y, Wei F (2014) Air filtration in the free molecular flow regime: a review of high-efficiency particulate air filters based on carbon nanotubes. Small 10:4543–4561. doi:10.1002/smll.201401553

Li Y, Wang J, Li X, Geng D, Li R, Sun X (2011) Superior energy capacity of graphene nanosheets for a nonaqueous lithium-oxygen battery. Chem Commun 47:9438–9440

Liu S, Tian J, Wang L, Sun X (2011) Microwave-assisted rapid synthesis of Ag nanoparticles/graphene nanosheet composites and their application for hydrogen peroxide detection. J Nanopart Res 13:4539–4548. doi:10.1007/s11051-011-0410-3

Liu X, Qin Z, Dou Z, Liu N, Chen L, Zhu M (2014) Fabricating conductive poly(ethylene terephthalate) nonwoven fabrics using an aqueous dispersion of reduced graphene oxide as a sheet dyestuff. RSC Adv 4:23869. doi:10.1039/c4ra01645a

Lopez R, Pascual M, Garcia-Sanoguera D, Sanchez-Nacher L, Balart R (2012) Improvement of liquid absorption properties of nonwoven polypropylene substrates by low pressure plasma treatment with CH4-O-2 mixture gas. Fiber Polym 13:1139–1144. doi:10.1007/s12221-012-1139-z

Man WS, Kan CW, Ng SP (2014) The use of atmospheric pressure plasma treatment on enhancing the pigment application to cotton fabric. Vacuum 99:7–11. doi:10.1016/j.vacuum.2013.04.018

Ramasundaram S, Jung JH, Chung E, Maeng SK, Lee SH, Song KG, Hong SW (2014) Increasing hydrophobicity of poly(propylene) fibers by coating reduced graphene oxide and their application as depth filter media. Carbon 70:179–189. doi:10.1016/j.carbon.2013.12.091

Shi C et al (2012) Monitoring influence of chemical preparation procedure on the structure of graphene nanosheets. Phys E 44:1420–1424. doi:10.1016/j.physe.2012.03.004

Singh BP, Nayak S, Nanda KK, Jena BK, Bhattacharjee S, Besra L (2013) The production of a corrosion resistant graphene reinforced composite coating on copper by electrophoretic deposition. Carbon 61:47–56. doi:10.1016/j.carbon.2013.04.063

Sun L, Yu H, Fugetsu B (2012) Graphene oxide adsorption enhanced by in situ reduction with sodium hydrosulfite to remove acridine orange from aqueous solution. J Hazard Mater 203–204:101–110. doi:10.1016/j.jhazmat.2011.11.097

Wang N, Wang X, Ding B, Yu J, Sun G (2012) Tunable fabrication of three-dimensional polyamide-66 nano-fiber/nets for high efficiency fine particulate filtration. J Mater Chem 22:1445–1452. doi:10.1039/c1jm14299b

Wang S, Dryfe RAW (2013) Graphene oxide-assisted deposition of carbon nanotubes on carbon cloth as advanced binder-free electrodes for flexible supercapacitors. J Mater Chem A 1:5279. doi:10.1039/c3ta10436b

Xiang C, Lu W, Zhu Y, Sun Z, Yan Z, Hwang C-C, Tour JM (2012) Carbon nanotube and graphene nanoribbon-coated conductive Kevlar fibers. ACS Appl Mater Interfaces 4:131–136. doi:10.1021/am201153b

Yang J et al (2012) 3D porous LiFePO 4/graphene hybrid cathodes with enhanced performance for Li-ion batteries. J Power Sources 208:340–344

Yoshida K, Matsukawa K, Imai M, Yano T (2009) Formation of carbon coating on SiC fiber for two-dimensional SiCf/SiC composites by electrophoretic deposition. Mater Sci Eng B-Adv 161:188–192. doi:10.1016/j.mseb.2008.11.032

Yue M et al (2015) Switchable hydrophobic/hydrophilic surface of electrospun poly (l-lactide) membranes obtained by CF4 microwave plasma treatment. Appl Surf Sci 327:93–99. doi:10.1016/j.apsusc.2014.11.149

Zhang J et al (2013a) Improved hydrophilicity, permeability, antifouling and mechanical performance of PVDF composite ultrafiltration membranes tailored by oxidized low-dimensional carbon nanomaterials. J Mater Chem A 1:3101–3111

Zhang J et al (2013b) Synergetic effects of oxidized carbon nanotubes and graphene oxide on fouling control and anti-fouling mechanism of polyvinylidene fluoride

ultrafiltration membranes. J Membr Sci 448:81–92. doi:10.1016/j.memsci.2013.07.064

Zhitomirsky I (1998) Electrophoretic and electrolytic deposition of ceramic coatings on carbon fibers. J Eur Ceram Soc 18:849–856. doi:10.1016/s0955-2219(97)00213-6

Zhou B et al (2015) Tailoring the chemical composition and dispersion behavior of fluorinated graphene oxide via CF4 plasma. J Nanopart Res 17:1–12. doi:10.1007/s11051-015-2946-0